

Solution of AGN accretion disk structure across a wide range of parameter space

Ho, Shing Chak Jeff

Winchester College, College St, Winchester SO23 9NA, United Kingdom

jeffho28@gmail.com

Abstract. Through the study of astrophysical accretion disks, considering the central role of angular momentum transport and energy conservation in determining the structure and evolution of accretion flow, we have constructed a comprehensive set of descriptions for the structure of accretion disks around supermassive black holes in active galactic nuclei (AGNs). The equation sets take into account various possible situations (gas pressure dominance, radiation pressure dominance, different heat production mechanisms, especially considering the latest research results on the turbulent heat production mechanism caused by gravity instability, etc.). By solving this system of equations, we give a general solution that covers multiple regions of a black hole's accretion disk. This will become an important tool for the community to effectively study other physical processes in the disk (such as the birth and evolution of stars, the diffusion of heavy elements, and the dynamical interactions of compact objects embedded in the disk).

Keywords: Black Holes, Accretion, AGN, Turbulence, MRI, Gravitational Instability.

1. Context

1.1. Introduction

Active galactic nucleus (AGN) is a small, compact and bright region in the center of a galaxy that has the highest luminosity. However, with the characteristics shown, the electromagnetic energy emitted was not produced by stars, instead, the radiation is produced by the accretion of matter around a central supermassive blackhole in the galaxy, which devours all matter that gets close to the region. The emitted radiation falls from a wide range of wavelengths, from radio waves to gamma rays, covering across the entire electromagnetic spectrum [1].

The cold matter accrete around the supermassive black hole is based on the conservation of angular momentum and mass. Despite the mass losing angular momentum as it falls into the center of the blackhole, there must be angular momentum transported outward of the black hole through turbulence, hence it redistributes and accretes the cold matter. The turbulence will also heat up the inner region of the disk, which is one of the variables that will be investigated in this paper. The most ubiquitous kind of turbulence that exists in the disk is caused by the Magnetorotational Instability (MRI) [2], which occurs as long as the disk is magnetized and satisfies:

$$\frac{d\Omega^2}{d \ln(R)} > 0 \quad (1)$$

$$\text{Where } v_{\text{orbital}} = \sqrt{\frac{GM}{R}} \quad (2)$$

Here Ω represents the Keplerian angular velocity of a fluid, and R represents the distance to the rotation centre.

In terms of the mechanism of momentum transport due to magnetic fields, it can be assumed that two arbitrary fluid elements on the inner region of an Keplerian disk can be acted as two mass points connected by a massless spring. The magnetic tension can simply be expressed as the spring tension of the massless spring. From the orbital velocity equation above, the inner fluid element will have a higher orbital velocity than the outer. This makes the ‘massless spring’ to stretch, the closer the region, the faster the orbital speed, the more restoring force there will be for the fluid element to slow down, decreasing the angular momentum. This process will cause the inner fluid element to move to a region with a smaller radius. On the other hand, from the conservation of momentum, the outer fluid element will have a greater angular momentum, and will be pulled outward to an orbit with a greater radius. This model shows that the spring constant in the ‘mass-spring system’ will increase as the two fluid elements move further apart, and gradually cause non-linear growth of perturbation.

In the outer regions of the AGN beyond a critical self-gravitating radius, the disk can also become cold and compact enough to develop gravitational instability or Jeans instability, where the disk tends to collapse vertically from its own self-gravity. The non-linear response from gravitational instability also causes turbulence, to a higher level than MRI such that it can heat the disk towards a marginally gravitationally stable state [3].

However, there is still a limit to the capability of gravito-turbulence in heating the disk against cooling, and beyond a second critical cooling radius, the turbulence/heating level reaches its maximum and runaway cooling is inevitable. In this scenario, the disk will fragment into self-gravitating clumps which leads to intense star formation, and the heat input from these stars may become the dominant heating source instead of turbulence to maintain the disk at a marginally self-gravitating quasi-steady state [4].

Due to different dominating turbulence and heating mechanisms, there are three main regions of the AGN disk, represented by different equations of structure and trends in the turbulent parameter α .

1.2. The Alpha Disk Model

The alpha disk model was proposed in 1973 by Shakura and Sunyaev [5], with the main property of being thermally and viscously unstable. Physical processes present in the disk leads to turbulence, where the turbulent viscosity of the disk is estimated as equation 3, where c_s is the speed of sound, and H is the scale height, which is represented by equation 4 through vertical hydrostatic equilibrium. Lastly, Ω is the Keplerian orbital angular velocity, calculated by equation 5, where M is the central mass of the supermassive black hole (SMBH), and R is the distance from its center.

$$\nu = \alpha c_s H \quad (3)$$

$$H = \frac{c_s}{\Omega} \quad (4)$$

$$\Omega = \frac{(GM)^{\frac{1}{2}}}{R^{\frac{3}{2}}} \quad (5)$$

There are a few factors to consider in the Alpha Disk Model. Consider an accretion disk that orbits in the $z = 0$ plane with polar coordinates (r, ϕ, z) . Assume that the disk is infinitesimally thin, with a negligible mass relative to its SMBH, and is hydrostatic balanced since it accretes slowly. If $z \ll r$, the density as a function of z can be written as, $\rho(z) = \rho_0 \left[-\frac{z^2}{2h^2} \right]$ for a nearly constant sound speed

(isothermal limit), which corresponds to the density ρ_0 at the disk at $z = 0$, the mid-plane point. From this relationship, the column integrated surface density, Σ , can be defined by equation 6, and the relation between the surface density and the density at mid-plane in equation 7.

$$\Sigma = \int_{-\infty}^{\infty} \rho(z) dz \quad (6)$$

$$\rho_0 = \frac{\Sigma}{fh} \quad (7)$$

In the isothermal limit the factor $f = \sqrt{2\pi}$, but we will generally apply $f = 2$, which holds approximately for any self-similar vertical profile. We will also use ρ to generally refer to the characteristic volume density of the disk.

The presence of viscosity is essential in producing heat when the $r\phi$ component of the stress tensor, $T_{r\phi}$, is present between two layers of differentially rotating fluid. This shear due to Keplerian differential rotation contributes to the transport of angular momentum around the SMBH, and can be estimated by equation 8. The product of ν and ρ , the density of the fluid, equals to the dynamic viscosity, μ . $T_{r\phi}$ can therefore be linked with viscosity by equation 8. By introducing an *ad hoc* assumption from dimensional analysis that the shear stress is proportional to the pressure of the accretion disk, where α is a turbulent viscosity parameter, shown in equation 9:

$$T_{r\phi} = \nu\rho r \frac{d\Omega}{dr} \approx \nu\rho\Omega \quad (8)$$

$$T_{r\phi} \sim \alpha P = \alpha\rho c_s^2 \quad (9)$$

We arrive at the ‘‘alpha description’’ equation 3.

Last but not least, the turbulence strength from a SMBH which is characterized by α provides a mass flux that accretes towards its center is denoted by \dot{M} , where:

$$\dot{M} = 3\pi\alpha c_s \Sigma H \quad (10)$$

This is a constant across distance in a quasi-steady state. The viscous dissipation also provides a heating rate per area, and can be derived by integrating the heating rate per unit volume in an accretion disk by a function of z . The heating rate per unit volume can be expressed by the surface density and the Keplerian shear stress on the $r\phi$ component:

$$q_+ = T_{r\phi} r \frac{d\Omega}{dr} = \mu \left(r \frac{d\Omega}{dr} \right)^2 = \frac{9}{4} \mu \Omega^2 \kappa \quad (11)$$

Integrating over z , the heating rate per unit surface area is:

$$Q_+ = \int_{-\infty}^{\infty} \frac{9}{4} \mu \Omega^2 \kappa dz = \frac{9}{4} \nu \Sigma \Omega^2 \kappa \quad (12)$$

In addition, while the disk cools by radiating from two surfaces at the effective temperature, T_{eff} , the temperature will decrease from the midplane due to optical depth τ in an optically thick environment.

$$T^4 = \frac{3}{8} T_{eff}^4 \tau = \frac{3}{8} T_{eff}^4 \kappa \Sigma \quad (13)$$

There is, however, a relation between effective temperature and Q_+ for optically thick cooling, where σ is the cross sectional area of interaction:

$$2\sigma T_{eff}^4 = \frac{9}{4} \nu \Sigma \Omega^2 \kappa \quad (14)$$

2. Mathematical Derivations

2.1. The Master Equation Sets and Three Disk Regions

Before giving a description of the model, there are some constants and variables that need to be defined. There are three equations sets for three main regions of the accretion disk, while some equations apply to more than one region.

- $\frac{\sigma_{SB}}{c} = a$, the radiation constant
- $\frac{k_B}{m_p} = \tilde{R}$, which is the molar gas constant
- σ_{SB} is the Stefan-Boltzmann constant
- $\kappa = \frac{\sigma}{\mu m_p}$ is the opacity, which we assume to be a constant in a high temperature region =

$0.4cm^2/g$ (electron scattering opacity). In the outer regions of the AGN the temperatures will drop below 10^4 - 10^3 K, and realistically the opacity will undergo a drop before settling down to the grain opacity $\sim 1 cm^2/g$. To first order we neglect this change and apply $\kappa = 0.4cm^2/g$ throughout our calculations.

Three equations can be formed by eliminating expressions for midplane density and scale height. The equations solve for the surface density, temperature and sound speed as functions of R , the distance from the center of the SMBH, if α is a constant. Extra care is needed in writing the equation of state (or pressure equation) since for hot regions of AGN disks, both radiation pressure

$$p_{rad} = \frac{aT^4}{3} \quad (15)$$

and ideal gas pressure

$$p_{gas} = \frac{\rho}{\mu} \tilde{R}T \quad (16)$$

needs to be taken into account. Here we take $\mu = 0.6$ for solar composition gas.

2.1.1. The First Disk Region. The first disk region has $Q > 1$, where Q is the Toomre's stability criterion. This criterion displays the relationship between parameters of a gaseous accretion disc that is differentially rotating to approximate its stability. With the shear force present, it can act as a stabilizing force, and when $Q > 1$, it means the system is stable against collapse.

This region is a hot disk that is gravitationally stable and heated by MRI turbulence. It has minimal turbulence, where the viscosity parameter is roughly a constant [5], with $\alpha = \alpha_{min} \sim 0.02$.

The equations below are the continuity, pressure and energy equation for this region:

$$\dot{M} = \frac{3\pi\alpha c_s^2 \Sigma}{\Omega} \quad (17)$$

$$\frac{\Sigma}{2c_s} c_s^2 = \frac{1}{3} aT^4 + \frac{\Sigma}{2c_s} \tilde{R}T \quad (18)$$

$$\frac{16\sigma_{SB}T^4}{3\kappa\Sigma} = \frac{9}{4} \left(\frac{\alpha c_s^2}{\Omega} \right) \Sigma \Omega^2 \quad (19)$$

2.1.2. The Second Disk Region. The second disk region is marginally gravitationally unstable, so Q is maintained to be a constant [3, 4]. The turbulence, α , adjusts to the cooling rate, so α is not a constant, and varies between α_{min} and α_{max} . This region has 4 equations that constrain 4 variables:

$$Q = 1, \text{ so } \frac{c_s \Omega}{\pi G \Sigma} = 1$$

$$\dot{M} = \frac{3\pi\alpha c_s^2 \Sigma}{\Omega} \quad (20)$$

$$\frac{\Sigma}{2c_s} c_s^2 = \frac{1}{3} a T^4 + \frac{\Sigma}{2c_s} \tilde{R} \frac{T}{\mu} \quad (21)$$

$$\frac{16\sigma_{\text{SB}} T^4}{3\kappa\Sigma} = \frac{9}{4} \left(\frac{\alpha c_s^2}{\Omega} \right) \Sigma \Omega^2 \quad (22)$$

2.1.3. *The Third Disk Region.* This region has a star-forming accretion disk, where its energy balance needs to be maintained by extra heating mechanisms, giving α takes its largest value. The extra heating needed to balance cooling is given by star formation so beyond the radius where $\alpha \sim \alpha_{\text{max}}$, the disk turbulence is decoupled from the energy equation. In this region, 3 equations and 3 variables apply:

$$Q = 1$$

$$\dot{M} = \frac{3\pi\alpha c_s^2 \Sigma}{\Omega} \quad (23)$$

$$\frac{\Sigma}{2c_s} c_s^2 = \frac{1}{3} a T^4 + \frac{\Sigma}{2c_s} \tilde{R} \frac{T}{\mu} \quad (24)$$

2.2. Limiting Solutions & General Remarks

Before we present the full numerical solutions that bridge all these regions, we would like to make some general remarks.

- Σ can be expressed by rearranging equation 24: $\Sigma = \frac{M\Omega}{3\pi\alpha c_s^2}$
- The generalized equation 25 can be re-written as $\frac{\Sigma}{2c_s/\Omega} c_s^2 = \frac{1}{3} a T^4$ in the radiation dominated region since $\frac{\Sigma}{2c_s/\Omega} \tilde{R} T/\mu$ is out of the limit.
- The equation of T^4 can be expressed after rearranging and by substituting Σ : $\frac{M\Omega^2}{2\pi\alpha c_s} = a T^4$
- The mass flow rate, \dot{M} , is a constant since the density profile remains unchanged.

The radiation dominated regime of the gravitationally stable region is at very close distance to the SMBH, where the following analytical solutions are presented:

Table 1. Solution A, Limited Solutions for the Gravitationally Stable Region.

<p>Equation of c_s from equation 19.</p>	$\frac{16\sigma_{SB}T^4}{3\kappa\Sigma} = \frac{9}{4}(\alpha c_s^2/\Omega)\Sigma\Omega^2$ $\frac{32\sigma_{SB}\dot{M}\Omega}{27\kappa\pi\alpha^2 c_s^3 a} = \Sigma^2$ $\frac{4\sqrt{6}\sigma_{SB}^{1/2}\dot{M}^{1/2}\Omega^{1/2}}{9\kappa^{1/2}\pi^{1/2}\alpha c_s^{3/2}a^{1/2}} = \Sigma$ $\frac{4\sqrt{6}\sigma_{SB}^{1/2}\dot{M}^{1/2}\Omega^{1/2}}{9\kappa^{1/2}\pi^{1/2}\alpha c_s^{3/2}a^{1/2}} = \frac{\dot{M}\Omega}{3\pi\alpha c_s^2}$ $c_s^{1/2} = \Omega^{1/2} \left[\frac{\dot{M}^{1/2} 9\kappa^{1/2} \pi^{1/2} \alpha a^{1/2}}{12\sqrt{6} \times \pi \alpha \sigma_{SB}^{1/2}} \right]$ $c_s = \Omega \left(\frac{3\dot{M}\kappa a}{32\pi\sigma_{SB}} \right) = \frac{3G^{1/2}M^{1/2}\dot{M}\kappa a}{32\pi\sigma_{SB}R^{3/2}}$
<p>Equation of T by using $\frac{\dot{M}\Omega^2}{2\pi\alpha c_s} = aT^4$:</p>	$T^4 = \frac{\dot{M}\Omega^2}{2\pi\alpha c_s}$ $T^4 = \frac{\dot{M}GMR^{-3/2}}{2\pi\alpha} \times \frac{32\pi\sigma_{SB}R^{3/2}}{3G^{1/2}M^{1/2}\dot{M}\kappa a}$ $T^4 = \frac{16\sigma_{SB}R^{3/2}G^{1/2}M^{1/2}}{3\alpha a^2\kappa R^3}$ $T^4 = \frac{16\sigma_{SB}G^{1/2}M^{1/2}}{3\alpha a^2\kappa R^{3/2}}$ $T = \frac{2\sigma_{SB}^{1/4}G^{1/8}M^{1/8}}{3^{1/4}\alpha^{1/4}a^{1/2}\kappa^{1/4}R^{3/8}}$
<p>Equation of Σ by using $\Sigma = \frac{\dot{M}\Omega}{3\pi\alpha c_s^2}$</p>	$\Sigma = \frac{\dot{M}}{3\pi\alpha} \times \frac{32^2\pi^2\sigma_{SB}^2R^3}{9GM\dot{M}^2\kappa^2a^2} \times \frac{G^{1/2}M^{1/2}}{R^{3/2}}$ $\Sigma = \frac{1024\pi\sigma_{SB}^2R^{3/2}}{27\alpha G^{1/2}M^{1/2}\dot{M}\kappa^2a^2}$

Table 1. (continued).

<p>Equation of ρ by using $\rho = \frac{\Sigma}{2H} = \frac{\Sigma\Omega}{2c_s}$</p>	$\rho = \frac{1024\pi\sigma_{SB}^2 R^{3/2}}{27\alpha G^{1/2} M^{1/2} \dot{M} \kappa^2 a^2} \sqrt{\frac{GM}{R^3}}$ $\times \frac{32\pi\sigma_{SB} R^{3/2}}{2 \times 3G^{1/2} M^{1/2} \dot{M} \kappa a}$ $\rho = \frac{32768\pi^2 R^3 \sigma_{SB}^3 M^{1/2} G^{1/2}}{162\alpha G M \dot{M}^2 \kappa^3 a^3 R^{3/2}}$ $\rho = \frac{16384\pi^2 \sigma_{SB}^3 R^{3/2}}{81\alpha G^{1/2} M^{1/2} \dot{M}^2 \kappa^3 a^3}$
<p>Equation of H by using $\rho = \frac{\Sigma}{2H}$</p>	$H = \frac{\Sigma}{2\rho}$ $H = \frac{1024\pi\sigma_{SB}^2 R^{3/2}}{27\alpha G^{1/2} M^{1/2} \dot{M} \kappa^2 a^2} \times \frac{81\alpha G^{1/2} M^{1/2} \dot{M}^2 \kappa^3 a^3}{2 \times 16384\pi^2 \sigma_{SB}^3 R^{3/2}}$ $H = \frac{27648 \dot{M} \kappa a}{29491 \sigma_{SB}}$

In this region, there are some properties displayed which can be verified graphically later. Since G , M , κ , α , π and σ_{SB} are constants, it can be deduced that $c_s \propto R^{-3/2}$, $T \propto R^{-3/8}$, $\Sigma \propto R^{3/2}$, $\rho \propto R^{3/2}$. The scale height is independent from the mass of the black hole and R , and the temperature is dependent on the mass flow rate.

As the distance from the center of the SMBH increases to the farthest limit, there is a point where we always enter the outermost star forming region, which introduces a new equation 25 for the region, and forms four new equations for c_s , Σ , T^4 and ρ , showing different trends.

$$\frac{c_s \Omega}{\pi G \Sigma} = 1 \tag{25}$$

Table 2. Solution B, Limited Solutions for the Star Formation Region.

$\frac{\dot{M}}{3\pi\alpha c_s^2} \Omega = \frac{c_s \Omega}{\pi G}$ $\frac{\dot{M}}{3\pi\alpha c_s^2} = \frac{c_s}{\pi G}$ $c_s^3 = \frac{\dot{M} G}{3\alpha}$ $c_s = \left(\frac{\dot{M} G}{3\alpha}\right)^{1/3}$	$\Sigma = \frac{c_s \Omega}{\pi G}$ $\Sigma = \frac{(\frac{\dot{M} G}{3\alpha})^{1/3} \Omega}{\pi G}$ $\Sigma = \frac{\dot{M}^{1/3} G^{-2/3} \times \sqrt{\frac{GM}{R^3}}}{3^{1/3} \alpha^{1/3} \pi}$ $\Sigma = \frac{\dot{M}^{1/3} M^{1/2} G^{-1/6}}{\sqrt[3]{3} \alpha^{1/3} \pi} R^{-3/2}$
--	---

Table 2. (continued).

$T^4 = \frac{3\Sigma\Omega c_s}{2a}$ $T^4 = \frac{3\Sigma\Omega c_s}{2a}$ $T^4 = \frac{3 \left(\frac{\dot{M}^{1/3} M^{1/2} G^{-1/6} R^{-3/2}}{\sqrt[3]{3}\alpha^{1/3}\pi} \right) \times \sqrt{\frac{GM}{R^3}} \times \left(\frac{MG}{3\alpha} \right)^{1/3}}{2a}$ $T^4 = \frac{\dot{M}^{2/3} MG^{2/3}}{2^3 \sqrt[3]{3}\alpha^{4/3}\pi} R^{-3}$ $T = \frac{\dot{M}^{1/6} MG^{1/6}}{2^{1/4} 3^{1/12} \pi^{1/4} \alpha^{1/3}} R^{-3/4}$	$\rho = \frac{\Sigma}{2H} = \frac{\Sigma\Omega}{2c_s}$ $\rho = \frac{\dot{M}^{1/3} M^{1/2} G^{-1/6}}{\sqrt[3]{3}\alpha^{1/3}\pi} R^{-3/2} \times \sqrt{\frac{GM}{R^3}}$ $\times \left(\frac{6\alpha}{MG} \right)^{1/3}$ $\rho = \frac{\sqrt[3]{6}\dot{M}^{1/3} MG^{1/3} M^{1/2} \alpha^{1/3}}{\sqrt[3]{3}\alpha^{1/3} R^3 \pi \dot{M}^{1/3} G^{1/3}}$ $\rho = \frac{\sqrt[3]{2}M}{R^3\pi}$
$H = \frac{\Sigma}{2\rho}$ $H = \frac{\dot{M}^{1/3} M^{1/2} G^{-1/6} R^{-3/2}}{\sqrt[3]{3}\alpha^{1/3}} \times \frac{R^3}{2^3 \sqrt[3]{2}M}$ $H = \frac{\dot{M}^{1/3} G^{-1/6} R^{3/2}}{2^3 \sqrt[3]{6} M^{1/2} \alpha^{1/3}}$	

In this region, the four sets of equations can show an accurate prediction on several properties of different variables in the region. Firstly, the speed of sound in the star formation disk is independent from R , meaning that it remains unchanged throughout the region. It is also unaffected by the mass of the black hole. Meanwhile, T and Σ has a steeper gradient in this region than the radiation dominated regime of the gravitationally stable region. Last but not the least, the volume density, ρ , is independent from both α and \dot{M} , meaning that the mass flow rate and the maximum turbulence does not affect ρ .

The limiting solutions above also show trends of the variables. For example, Σ and ρ will generally increase in the inner region and decrease in the outer region against R . T will decrease continuously but at two different rates. c_s will decrease at the start and then become a constant in the star forming region. Last but not least, the scale height, H , is a constant in the radiation domination region, and then increases after.

2.2.1. Radiation vs. Gas Pressure Ratio. The radiation/gas pressure ratio is denoted by $\Pi = \frac{p_{rad}}{p_{gas}} =$

$$\frac{aT^4/3}{\frac{E_{RT}}{\mu}} \propto \frac{T^3}{\rho}$$

In the inner solution, since $T \propto R^{-3/8}$ and ρ is independent of R , as the distance from the center increases in the region, the radiation pressure/gas pressure will decrease. However in the outer solution, $T^3 \propto R^{-9/4}$ and $\rho \propto R^{-3}$, which makes Π to be proportional to $R^{3/4}$, hence the radiation pressure/gas pressure will increase across the region. This gives a conclusion that there is a transition region which is sandwiched in between the two regions, where radiation pressure vs gas pressure ratio reaches a minimum and the scaling for temperature/density diverges from these limiting solutions. This will be also tested graphically below.

3. Numerical Solutions

3.1. The Fiducial Case

Full numerical solution for the fiducial case, across different disk regions, is shown with black lines in Figure 3. The parameters are defined as shown:

$$\dot{M} = \frac{M_{\odot}}{yr} \quad (26)$$

$$M = 10^8 M_{\odot}$$

$$\alpha_{min} = 0.01$$

$$\alpha_{max} = 0.3$$

The most inner region of the SMBH is gravitationally stable, and it is entirely heated by MRI turbulence, with α_{min} as a constant at approximately 0.02. With low turbulence, there are some properties displayed in this region which conforms with our solution A) in section 2.2. The scale height, H , remains constant against R , and the volume density and surface density both have a steady increase until it reaches gravitational instability. However, from $\frac{3}{4}$ the way out from the gravitational stable region, the rate of increase in surface density slows down, which displays another trend when gas pressure begins to take dominance, but before this transition is complete the disk enters the marginally gravitationally unstable region at ~ 0.01 pc.

The disks in the gravitational instability region 2 is heated mainly the gravito-turbulence, where the value of α varies in the range $\alpha_{min} < \alpha < \alpha_{max}$. It has a value of $Q = 1$, full equation displayed in equation 25. This shows that the turbulence can change to accommodate the radiative cooling rate in order to maintain the Q value. Figure 1 shows that the α increases steeply as the distance from the disk to the center of the SMBH increases in this region between ~ 0.01 pc and 0.3pc.

In addition, through Figure 3 it shows that as the disk approaches the gravitationally unstable region, there is a continued decline in the ratio of radiation pressure to gas pressure. This indicates that their values are approaching to be equal, and eventually reaches the minimum at the transition to the third region at ~ 0.3 pc. The scalings are slightly nonlinear because gas pressure and radiation pressure are comparable to each other.

Approaching this radius beyond the point where $\alpha \sim \alpha_{max}$, the disk will fragment and form stars. The turbulence will reach its highest level, where the α value is fixed at α_{max} . Then cooling remains more efficient than the heating sector, mainly due to the turbulence parameter remaining constant. The outer region is where star formation occurs, hence the stars provide heat. There are several properties that conform to the solution B) in section 2.2 in this region, such as the sound speed converges to a constant, since it is independent of R , and both the surface and volume density decreases linearly as R increases.

3.2. Dependence on \dot{M} & M

We vary the mass flux and mass of the black hole by an order of 10 to observe the changes of disk profile depending on these two parameters. Four cases with $\dot{M} = [0.1, 10] \frac{M_{\odot}}{yr}$ and $M = [0.1, 10] \times 10^8 M_{\odot}$ are plotted together with the fiducial cases in Figure 2. The labels indicate their “ \dot{M} ” (accretion rate) and “ M ” (SMBH mass) ratio with the fiducial case, respectively e.g., $Md_1_M_10$ means the same accretion rate as the fiducial case but a 10 times larger SMBH mass.

First of all, changing the mass of the black hole changes the location of the star formation disk from the center of the SMBH, and Figure 3 shows that the greater the mass of a black hole, the further away the star formation disk is, and vice versa. As the limiting equations from section 2.2 shows that c_s is independent from R in the star formation region, the point on the graph where c_s starts to be constant and can determine its location. For instance, after increasing the mass of the black hole by a factor 10, the point where c_s becomes constant changes from ~ 0.3 pc to ~ 0.55 pc. In addition, changing the mass

and mass flux also impacts the magnitude of the speed of sound, where changing the mass flux makes greater change in c_s . From the equation in section 2.2, If R is constant, then the sound speed is proportional to $M^{1/2}$ and \dot{M} , therefore the equations conform with the graph shown.

The surface density has similar trends with the volume density, where when the mass flux (accretion rate) is lower, there tends to have a slower increase against R at the gravitational stable disk. The densities all reach their maximum at the point right before entering the star formation disk, and decrease linearly after that, which conforms to the two limiting equations. Figure 3 shows that the surface density changes slightly more when the mass of the black hole is changed than its mass flux, and this matches with the limiting equations, as it shows that Σ is proportional to $M^{-1/2}$ or \dot{M} assuming if all other variables are constant. However, surface density and volume density both decrease at the same rate in the star forming region, no matter if the black hole has a different mass flux or mass. The mass flux does not have any impact in the volume density of a black hole in the same region as the equation does not have \dot{M} , and this corresponds to the Solution B) in section 2.2.

The scale height is independent from the mass of the black hole in the gravitationally stable disk, and this is shown in Solution A), which matches with the graph in Figure 3. The graph shows that black holes with mass by a scale factor of 0.1 and 10 from the normal one all have the same scale height from the center of the SMBH until they approach the gravitationally unstable region and they start to separate and increase non-linearly. However, the scale height at very large distances increases linearly and at the same rate for all black holes shown on the graph with different mass fluxes or masses, though it is greater for black holes with greater mass flux or smaller mass. This matches with the limiting solutions, as the scale height is proportional to $\dot{M}^{1/3}$ and $M^{-1/2}$.

The temperature profile mildly increases with larger \dot{M} and M , but the scalings are non-linear in the middle regions. It is close enough to the SMBH where profiles converge to Solution A) in section 2.2, the temperature converges to the profile for different \dot{M} , and only has a mild positive correlation with M . Last but not the least, Figure 3 shows that the radiation vs. gas pressure ratio decreases at a constant rate at the start, and then at a different gradient in the gravitational unstable disk, then at the point of reaching a minimum, it increases non-linearly since it enters the star formation disk, which is radiation dominated. The trend and graphics correspond with the conclusions stated earlier, which states that the gas pressure and radiation pressure is approximately equal in the transition region between the gravitationally stable and the star formation region.

3.3. Dependence on α_{max}

There are recent radiation hydrodynamic simulations that suggest the maximum level of turbulence supported by gravitational instability in disks with non-negligible radiation pressure ($> \sim 10\%$) is not as large as gas-only simulations previous literature suggests and may be as low as 0.02 [6]. We have tested α_{max} at three different values (0.3, 0.1, 0.02) for $M = 10^8$ and $\dot{M} = 0.1$, and observe how they depend on the maximum turbulence. The default maximum turbulence is $\alpha_{max} \sim 0.3$. There are some remarkable trends which are observed, and noticeable changes occur from the start of the star formation disk. The temperature continuously decreases as we go further away from the center of a SMBH, however, as it reaches the star formation disk, the temperature decreases at a faster rate, and different maximum turbulence changes the initial temperature at the disk. The lower maximum turbulence, the higher temperature at a certain R , however the turbulence does not affect the rate of the temperature drop as R increases.

There are also some similar trends which show that the transition from the gravitationally unstable disk to the star-forming disk is closer with a lower maximum turbulence. For example, the sound speed evidently shows that it approaches zero gradient in a lower R value at $\alpha_{max} = 0.02$ at $r \sim 0.01 pc$ while at $\alpha_{max} = 0.3$, the gradient turns zero at $r \sim 0.05 pc$. This property also matches to the graphs with other parameters, such as the surface density and the scale height as the gradient changes later for higher α_{max} values. The volume density, however, has the same values throughout the SMBH, unaffected by the maximum turbulence, which conforms with the equations in Sec. 2. Last but not least,

the radiation vs. gas pressure ratio also conforms with the conclusions from the limited solutions, which shows that there is a minima which is sandwiched between the gravitational unstable region and the star formation region. It also matches the trend where lower turbulence limit corresponds to a smaller transition region, as the graphs also shows that star formation region begins at $r \sim 0.01 pc$ when $\alpha_{max} = 0.02$, and $r \sim 0.05 pc$ when $\alpha_{max} = 0.3$. We do expect there to be no region 2 if $\alpha_{max} = \alpha_{min}$.

Because the onset of star formation (or the limit on turbulence parameter) reverses the trend of radiation to gas pressure fraction with respect to radius, an early transition to region 3 at larger radiation pressure fraction (for our low α_{max} values) suggests that the disk may simply not be able to reach low enough radiation pressure fraction in order for a gas pressure supported disk to provide larger levels of turbulence, therefore the low α_{max} solutions will be more realistic.

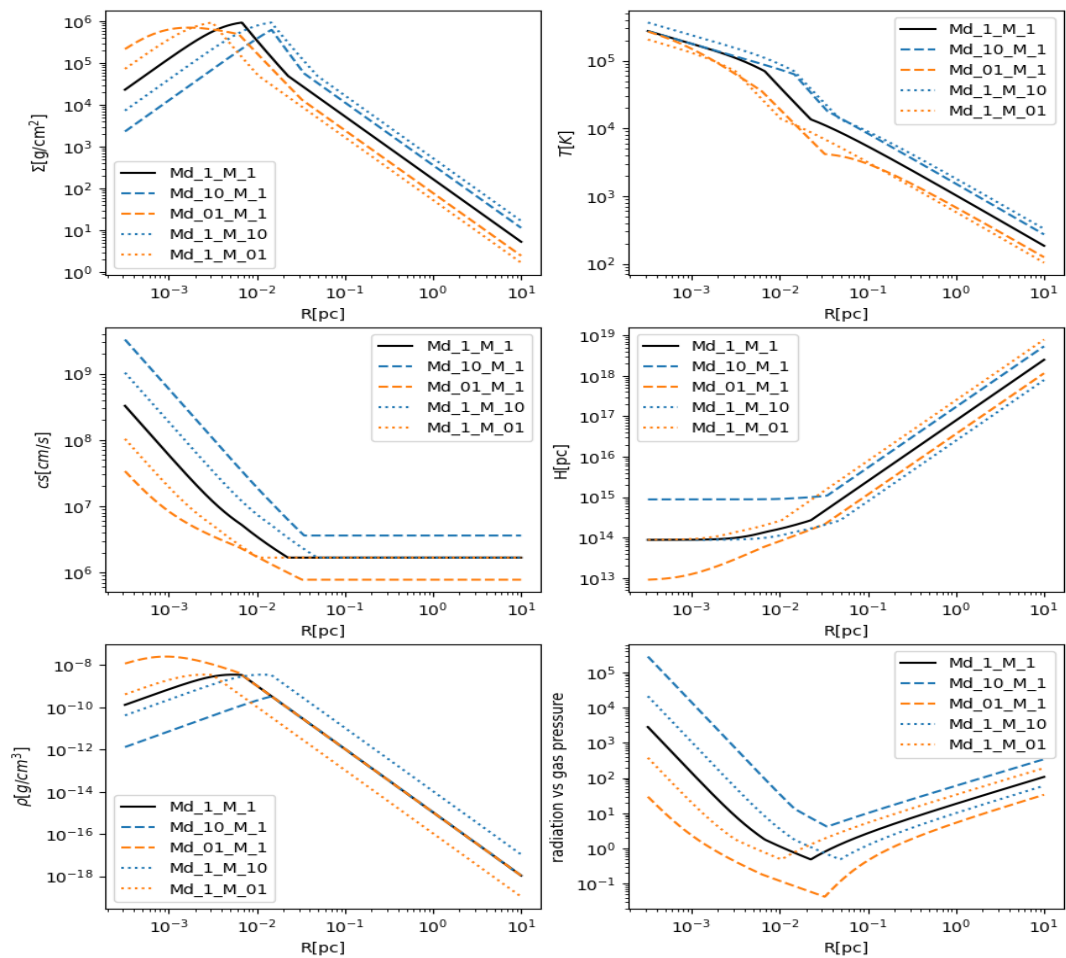


Figure 1. Corresponding Graphs for Different Parameters Against the Distance from the Center of SMBHs with Different Accretion Rates.

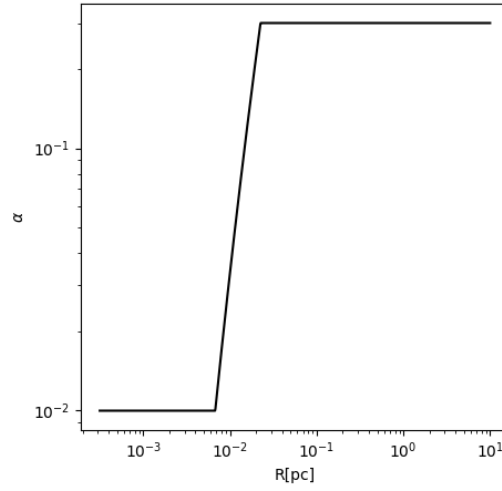


Figure 2. Graph of the Turbulence Constant, α , against the Distance from the SMBH Center.

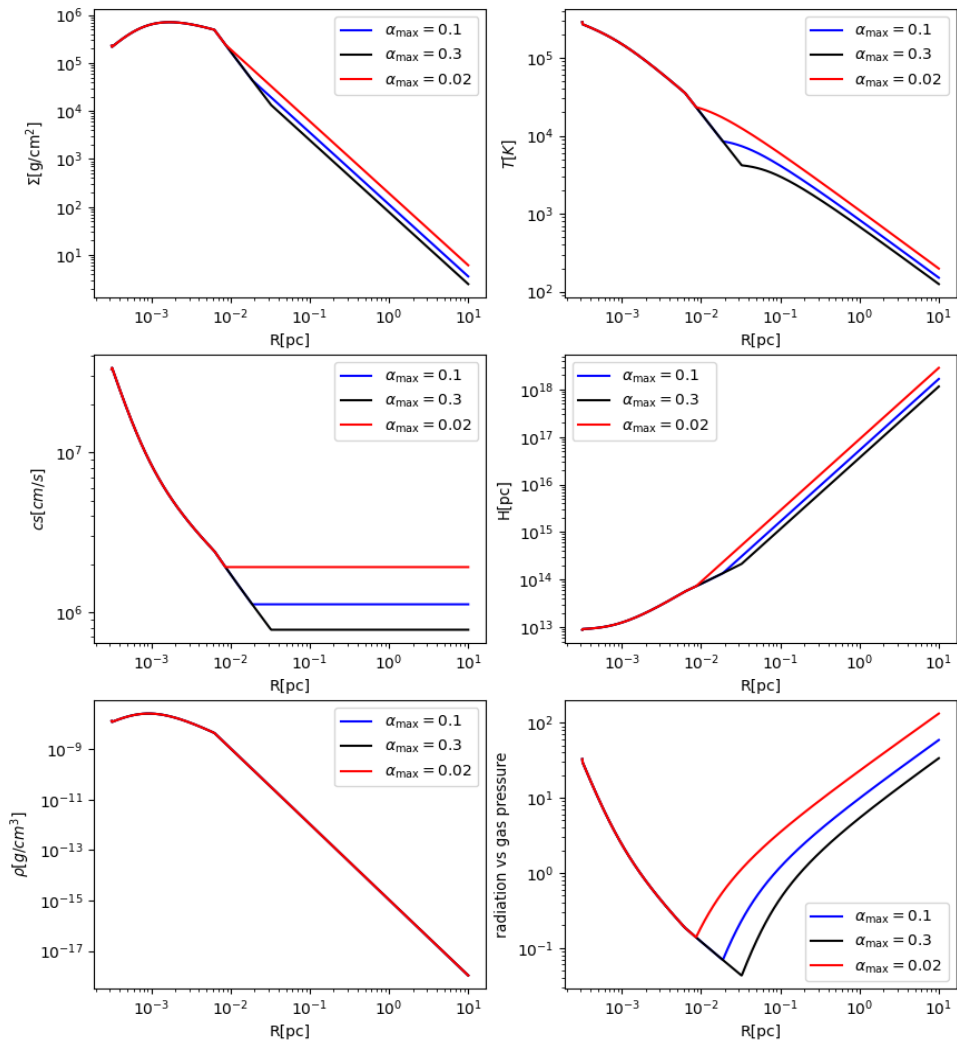


Figure 3. Corresponding Graphs for Different Parameters Against the Distance from the Center of SMBHs with Different Maximum Turbulences.

4. Further Applications

Our disk models can be applied to the modeling of multiple scenarios. First of all, the modeling is directly useful for understanding different temperature profiles of AGN accretion disks probed by reverberation mapping observation [7], and discussing what processes resulted in different dependencies of surface temperature with respect to distance R . Secondly, a disk of stars in the galactic center with a low mutual inclination is suggested to originate from gravitational collapse in an accretion disk while Sgr A* was still in an active phase [8, 9]. In this case, our AGN solutions effectively map out regions of star formation for accretion disk of any M and M_* , and can be used to study the properties of the fragments or proto-stars as functions of R in the galactic center as well as in the outskirts of other AGNs.

In addition, another strong evidence for star formation in AGNs lies in the metallicities measured in AGNs. If the metallicities in AGNs are the same as their background environment, it should become more metal poor or “younger” when redshift increases. However, observation of line ratios in AGN spectra show their super-solar abundances do not vary with redshift [10, 11]. This means that stars born in AGNs can pollute their environment through their evolution off the main sequence and their supernovae. Therefore, understanding the disk structure can be useful in calculating the diffusion of elements from embedded stars and how they enhance the metallicity of the whole accretion disk.

Lastly, massive black hole merger components detected in LIGO mergers have been proposed to be of AGN origin [12, 13]. A stellar-mass black hole with approximately 10 solar masses can quickly grow to 30-50 solar mass in an AGN disk either from accreting gas or frequent mergers with their neighbors. This process takes place in the AGN origin, as it is highly dense, lots of stars and black holes can be formed, hence collisions known as galaxy merger occur. In such circumstances, understanding accurate disk structures are crucial in our understanding of the swarm of black holes' migration and dynamical interaction with the accretion disk, and their thermal feedback onto the disk, in order to predict distinct features of LIGO sources produced from the AGN channel.

5. Conclusions

In this paper, we developed a numerical framework to conveniently generate AGN disk profiles across a wide distance and parameters space, by specifying basic inputs like M , M_* , α_{max} , α_{min} , and the opacity. Starting from the center of the SMBH, enters the innermost region where the disk will be radiation dominated, and gravitationally stable heated by MRI, to a radiation-dominated, star formation region in the outermost parts. Meanwhile, the middle region displays a minimum of radiation pressure fraction and gravito-turbulence heating which may prevent star formation. We have provided full analytical solutions to the two (closest and furthest) limits of the SMBH, which are verified by numerical solutions of AGN disk that also include the non-linear transition between these two limits. They will be useful in studies of physical processes in AGNs that require modeling of the AGN disk structure.

Acknowledgements

Early this summer, I attended the Astro1107 course in Cornell SCE Pre College Studies; the lectures led by Professor David A. Kornreich have enhanced my background knowledge to complete this research and skills to write a scholarly research paper. I would like to thank my mentor, Mr. Yixian Chen, for encouraging and guiding me in writing this paper and offering me professional advice on using computer programming to display the solutions visually. I also thank his patience and help guiding me through complex Mathematical proofs behind the theories. I would also like to thank my supervisor, Mr. Jeremy Douglas, my Physics teacher at Winchester College, for giving me valuable feedback and continuously challenging my understanding when writing the paper.

References

- [1] Lynden-Bell, D. (1969). Galactic Nuclei as Collapsed Old Quasars. *Nature*, 223(5207).
- [2] Balbus, S. A. (2003). Enhanced angular momentum transport in accretion disks. *Annual Review of Astronomy and Astrophysics*, 41(1), 555-597.

- [3] Gammie, C. F. (2001). Nonlinear outcome of gravitational instability in cooling, gaseous disks. *The Astrophysical Journal*, 553(1), 174.
- [4] Thompson, T. A., Quataert, E., & Murray, N. (2005). Radiation pressure-supported starburst disks and active galactic nucleus fueling. *The Astrophysical Journal*, 630(1), 167.
- [5] Shakura, N. I., & Sunyaev, R. A. (1973). Black holes in binary systems. Observational appearance. *Astronomy and Astrophysics*, Vol. 24, p. 337-355, 24, 337-355.
- [6] Chen, Y., Jiang, Y., Goodman, J., & Ostriker, E. (2023). 3D Radiation Hydrodynamic Simulations of Gravitational Instability in AGN Accretion Disks: Effects of Radiation Pressure. *The Astrophysical Journal*, 948(2), 120
- [7] Cackett, E. M., Bentz, M. C., & Kara, E. (2021). Reverberation mapping of active galactic nuclei: From X-ray corona to dusty torus. *Iscience*, 24(6).
- [8] Levin, Y., & Beloborodov, A. M. (2003). Stellar disk in the galactic center: a remnant of a dense accretion disk?. *The Astrophysical Journal*, 590(1), L33.
- [9] Paumard, T., Genzel, R., Martins, F., Nayakshin, S., Beloborodov, A. M., Levin, Y., ... & Sternberg, A. (2006). The two young star disks in the central parsec of the galaxy: properties, dynamics, and formation. *The Astrophysical Journal*, 643(2), 1011.
- [10] Hamann, F., & Ferland, G. (1999). Elemental abundances in quasistellar objects: star formation and galactic nuclear evolution at high redshifts. *Annual Review of Astronomy and Astrophysics*, 37(1), 487-531.
- [11] Nagao, T., Marconi, A., & Maiolino, R. (2006). The evolution of the broad-line region among SDSS quasars. *Astronomy & Astrophysics*, 447(1), 157-172.
- [12] McKernan, B., Ford, K. E. S., Lyra, W., & Perets, H. B. (2012). Intermediate mass black holes in AGN discs–I. Production and growth. *Monthly Notices of the Royal Astronomical Society*, 425(1), 460-469.
- [13] McKernan, B., Ford, K. E. S., Kocsis, B., Lyra, W., & Winter, L. M. (2014). Intermediate-mass black holes in AGN discs–II. Model predictions and observational constraints. *Monthly Notices of the Royal Astronomical Society*, 441(1), 900-909.
- [14] Ali-Dib, M., Cumming, A., & Lin, D. N. (2020). The imprint of the protoplanetary disc in the accretion of super-Earth envelopes. *Monthly Notices of the Royal Astronomical Society*, 494(2), 2440-2448.

Appendix A: Derivations on Gas Dominated Region 1

Starting from equation 19, we can solve analytically in the radiation dominated limit which results in solution A in section 2.2. With a relatively lower temperature, the disk can become gas pressure dominated at the outer parts in the first region before transitioning to region 2 in certain parameter space. In this process, the pressure equation is simplified to:

$$T = \frac{\mu c_s^2}{\bar{R}} \quad (A1)$$

To find the trend of sound speed, surface density and temperature of the accretion disk against the distance from the center of the SMBH, the proportionality between the two variables need to be found. In the gas dominated region, it is known that equation 24 holds.

Meanwhile, equation A1 only holds when gas pressure dominates.

● To find the relationship between the sound speed and the distance from the black hole, variables such as Σ and T has to be eliminated. From equation 24, the surface density can be written in terms of $\Sigma = \frac{\dot{M}}{3\pi\alpha c_s^2} \Omega$. Then, substitute it in equation 19, making:

$$\frac{9}{4(\alpha c_s^2) \left(\frac{\dot{M}}{3\pi\alpha c_s^2} \right) \Omega^2} = \frac{16\sigma_{SB} T^4 (3\pi\alpha c_s^2)}{3\kappa(\dot{M}\Omega)} \quad (A2)$$

T can then be eliminated by substituting equation A1 into A2:

$$\begin{aligned} \frac{3}{4}(\alpha c_s^2)\left(\frac{\dot{M}}{\pi\alpha c_s^2}\right)\Omega^2 &= \frac{16\sigma_{SB}\mu^4 c_s^4(3\pi\alpha c_s^2)}{3\tilde{R}^4\kappa(\dot{M}\Omega)} \\ \frac{1}{4\pi}\dot{M}\Omega^2 &= \frac{16\sigma_{SB}\mu^4 c_s^4(\pi\alpha c_s^2)}{3\tilde{R}^4\kappa(\dot{M}\Omega)} \\ \frac{1}{4\pi}\dot{M}\Omega^2\left(\frac{\dot{M}\Omega}{\pi\alpha c_s^2}\right) &= \frac{16\sigma_{SB}\mu^4 c_s^4}{3\tilde{R}^4\kappa} \\ \frac{\dot{M}^2\Omega^3}{4\pi^2\alpha c_s^2} &= \frac{16\sigma_{SB}\mu^4 c_s^4}{3\kappa\tilde{R}^4} \\ c_s^{10} &= \frac{3\kappa\tilde{R}^4\dot{M}^2\Omega^3}{64\pi^2\alpha\sigma_{SB}\mu^4} \end{aligned}$$

Then, eliminate Ω by substituting it with equation 1.5:

$$c_s^{10} = \frac{3\kappa\tilde{R}^4\dot{M}^2 G^{3/2} M^{3/2}}{64\pi^2\alpha\sigma_{SB}\mu^4 R^{9/2}}$$

Since the other variables are all constants, the proportionality between sound speed and distance from the center of the SMBH is computed: $c_s \propto R^{-9/20}$

● For the relationship between temperature T and the distance, equation 24 can be used:

$$T = \frac{\mu c_s^2}{\tilde{R}} \text{ and since } \frac{\mu}{\tilde{R}} \text{ is a constant,}$$

$T \propto c_s^2$, which gives the final proportionality, where $T \propto R^{-9/10}$

● Using equation 25, the relationship between the surface density of the disk Σ and the distance can be found:

$$\Sigma = \frac{\dot{M}}{3\pi\alpha c_s^2}\Omega, \text{ since } \frac{\dot{M}}{3\pi\alpha} \text{ is a constant and } \Omega \text{ is dependent on } R^{-3/2},$$

$\Sigma \propto \frac{R^{-3/2}}{R^{-9/10}}$, which gives the final proportionality, where $\Sigma \propto R^{-3/5}$

This branch of solution does not appear for all our accretion rate and SMBH mass parameters since some of them become gravitationally unstable within the radiation dominated part already. However, this solution does coincide with the solution for a viscously heated inner part of a protoplanetary disk [14].